Magnetic Microstructures of Nano-Granular CoPt-Al-O Thin Films Studied by Lorentz Microscopy and Electron Holography

doi: 10.1109/TMAG.2005.854674

Magnetic Microstructures of Nano-Granular CoPt–Al–O Thin Films Studied by Lorentz Microscopy and Electron Holography

H. S. Park[1], D. Shindo[1], S. Mitani[2], and K. Takanashi[2]

[1]Institute of Multidisciplinary Research for Advanced Materials, Tohoku University, Sendai 980-8577, Japan
[2]Institute of Materials Research, Tohoku University, Sendai 980-8577, Japan

Microstructures and magnetic domain structures of nano-granular CoPt–Al–O thin films are investigated by Lorentz microscopy and electron holography. It is found that the CoPt-based nanocrystalline phases are basically surrounded by the Al_2O_3-based amorphous phases and the area of the Al_2O_3-based amorphous phases increases with the increase in oxygen content. Typical mazy domains and domain walls like fishbone are observed in the $Co_{45.8}Pt_{18.6}Al_{17.3}O_{18.3}$ and in localized area of the $Co_{38.7}Pt_{15.6}Al_{16.3}O_{29.4}$, respectively, while no magnetic domain walls are observed in the $Co_{34.4}Pt_{13.5}Al_{15.6}O_{36.5}$. With the increase in magnetic field, domain walls like fishbone start to disappear and the magnetic flux density increases in the $Co_{38.7}Pt_{15.6}Al_{16.3}O_{29.4}$, indicating the mixed-phase state of ferromagnetic and superparamagnetic phases. In the $Co_{34.4}Pt_{13.5}Al_{15.6}O_{36.5}$ of superparamagnetic state, the fluctuated lines of magnetic flux are considered to reflect the randomly magnetized distribution of CoPt-based single domain particles.

***Index Terms*—Electron holography, lines of magnetic flux, magnetic domain structure, nano-granular thin film.**

I. Introduction

NANO-GRANULAR magnetic films have attracted much attention for their unique magnetic properties, i.e., high-frequency soft and high-anisotropy magnetic properties and giant magnetoresistance (GMR) effect [1]–[3]. Thus, nano-granular magnetic films have recently been in increasing demand for use in various electronic devices such as high-frequency magnetic devices, ultrahigh density recording media, and magnetic sensors [4]. It is well known that the microstructures of nano-granular films depend sensitively on the oxygen content, i.e., the volume fraction of the nanocrystalline phase with respect to the amorphous phase. For example, the nano-granular Co–Al–O thin films show the soft ferromagnetic and superparamagnetic states, depending on the partial pressure of O_2 gas for sputtering. Further, a pronounced GMR was found in Co–Al–O superparmagnetic films, exhibiting large MR values of about 8% under an applied magnetic field of 960 kA/m at room temperature [2], which was originated from the spin-dependent tunneling effect.

In order to further improve the magnetic properties of nano-granular thin films, understanding the microstructures and magnetic domain structures is of vital importance. Thus far, the correlation between the magnetic properties and the microstructures has been investigated by a few research groups, using high-resolution transmission electron microscopy (HRTEM) and small-angle X-ray scattering (SAXS) [3], [5]. However, the observation of magnetic domain structures in nano-granular thin films has been hardly carried out especially under the applied magnetic fields, although it is requisite for both fundamentals and applications of nano-granular thin films. In this paper, the microstructures and magnetic domain structures in various CoPt–Al–O thin films are analyzed in detail by utilizing HRTEM, Lorentz microscopy, and electron holography. Under the applied magnetic fields, the change in magnetic domain structures of $Co_{38.7}Pt_{15.6}Al_{16.3}O_{29.4}$ thin film is briefly discussed.

TABLE I
Electrical Properties of CoPt–Al–O Thin Films

Specimen	Electrical resistivity	Property
$Co_{45.8}Pt_{18.6}Al_{17.3}O_{18.3}$	2×10^{2} $\mu\ \Omega$cm	AMR
$Co_{38.7}Pt_{15.6}Al_{16.3}O_{29.4}$	2×10^{3} $\mu\ \Omega$cm	TMR 1 %
$Co_{34.4}Pt_{13.5}Al_{15.6}O_{36.5}$	$>10^{5}$ $\mu\ \Omega$cm	TMR 3 %

[a]AMR and TMR indicate the anisotropy magnetoresistance and tunneling magnetoresistance, respectively.

II. Experimental Procedure

Three kinds of CoPt–Al–O thin films with different compositions were prepared on glass substrates by a reactive sputtering in an Ar+O_2 atmosphere. Some of their electrical properties are presented in Table I. The composition of specimens was analyzed by energy dispersive X-ray spectroscopy (EDS). The thin foil specimens for TEM observations were prepared by one-side grinding and Ar ion milling (glass substrate side) and subsequently both sides milling to remove the surface contamination. Microstructures were studied using a JEM-3010 TEM operated at 300 kV.

In situ observations with Lorentz microscopy and electron holography were carried out using a JEM-3000F TEM with a field emission gun and a biprism. This microscope has a special polepiece designed for observing the magnetic domains; that is, the magnetic field at the specimen position can be reduced to 1.6 kA/m [6]. Reconstructed phase images of the holograms were obtained from the digitized holograms with the Fourier transform. The phase shift $\phi(x, y)$ due to the magnetic field of the specimens is represented by $\cos\phi(x, y)$ in the reconstructed phase images, as described elsewhere in detail [7]. The change

Digital Object Identifier 10.1109/TMAG.2005.854674

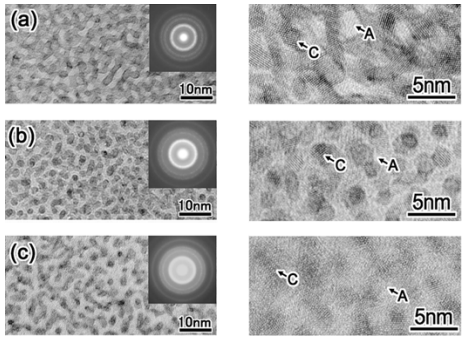

Fig. 1. TEM and high-resolution TEM images of (a) $Co_{45.8}Pt_{18.6}Al_{17.3}O_{18.3}$, (b) $Co_{38.7}Pt_{15.6}Al_{16.3}O_{29.4}$, and (c) $Co_{34.4}Pt_{13.5}Al_{15.6}O_{36.5}$ thin films. A and C indicate the amorphous phase and crystalline phase, respectively.

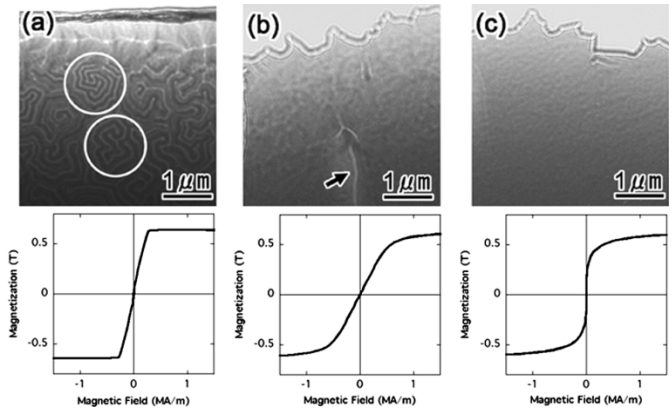

Fig. 2. Lorentz microscope images (upper parts) and magnetization curves (lower parts) of (a) $Co_{45.8}Pt_{18.6}Al_{17.3}O_{18.3}$, (b) $Co_{38.7}Pt_{15.6}Al_{16.3}O_{29.4}$, and (c) $Co_{34.4}Pt_{13.5}Al_{15.6}O_{36.5}$ thin films. The magnetization was measured in the thin film plane.

in magnetic domains and lines of magnetic flux is studied with a magnetic holder that can produce a maximum magnetic field of about 16 kA/m within a TEM.

III. Results and Discussion

Fig. 1 shows bright-field TEM images with the corresponding electron diffraction patterns and HRTEM images of (a) $Co_{45.8}Pt_{18.6}Al_{17.3}O_{18.3}$, (b) $Co_{38.7}Pt_{15.6}Al_{16.3}O_{29.4}$, and (c) $Co_{34.4}Pt_{13.5}Al_{15.6}O_{36.5}$ thin films. Debye–Scherrer rings in diffraction patterns become sharper with the increase in Co content, indicating the existence of the nanocrystalline phases. Since the bright regions become larger with the increase in O content [Fig. 1(b) and (c)], the bright and dark regions are considered to correspond to the Al_2O_3-based amorphous phases and CoPt-based nanocrystalline phases, respectively. From HRTEM analysis, it is found that in Fig. 1(b) and (c), the nanocrystalline phases are basically surrounded by the amorphous phases, showing the nano-granular structures. In contrast, the nanocrystalline phases are interconnected and surround the amorphous phases in Fig. 1(a), resulting from the volume fraction of the nanocrystalline phases exceeding the percolation limit. It is noted that the $Co_{45.8}Pt_{18.6}Al_{17.3}O_{18.3}$ shows the small electrical resistivity of 2×10^2 $\mu\Omega$·cm. Therefore, in the $Co_{45.8}Pt_{18.6}Al_{17.3}O_{18.3}$, the electrical conduction is considered to be governed by metallic conduction.

Fig. 2 shows Lorentz microscope images (upper parts) and magnetization curves (lower parts) of (a) $Co_{45.8}Pt_{18.6}Al_{17.3}O_{18.3}$, (b) $Co_{38.7}Pt_{15.6}Al_{16.3}O_{29.4}$, and (c) $Co_{34.4}Pt_{13.5}Al_{15.6}O_{36.5}$ thin films, which were observed with the Fresnel mode under the defocused condition. Typical mazy domain structures are observed in the lower thick regions of Fig. 2(a), being prominent in such regions with the antiparallel magnetization vector perpendicular to thin film. This observation is consistent with the magnetization curve of $Co_{45.8}Pt_{18.6}Al_{17.3}O_{18.3}$, where the perpendicular anisotropy field (effective field inducing demagnetizing effect) is evaluated to be approximately 240 kA/m. However, in the upper thin regions of Fig. 2(a), the cross-tie walls can be seen. Except such thin regions where the magnetization vector almost lies in the thin film plane except some Bloch lines [8], typical mazy domains can be seen. Comparing the two white-circled regions in Fig. 2(a), the domain width D tends to increase with the increase in specimen thickness t. This seems to be basically consistent with the form of a power dependence $D(t) = at^b$ [9], [10], where a and b are the constants. Detailed analysis of domain width D as a function of thickness t will be studied elsewhere. In the $Co_{38.7}Pt_{15.6}Al_{16.3}O_{29.4}$ of Fig. 2(b), domain walls like fishbone indicated by the black arrow are observed in localized area, which was also observed in nano-granular Co-Zr-O thin films [11]. On the other hand, no magnetic domain walls are observed in the $Co_{34.4}Pt_{13.5}Al_{15.6}O_{36.5}$ of Fig. 2(c). Although there is a faint contrast in Fig. 2(c), it is considered that such a faint contrast results from the specimen surface roughness.

Fig. 3 shows Lorentz microscope images (left parts) and the reconstructed phase images (right parts) of $Co_{38.7}Pt_{15.6}Al_{16.3}O_{29.4}$ thin film obtained when the magnetic fields applied are 0, 1.6, 4.8, and 11.2 kA/m, respectively. The holograms were obtained from the rectangle in Fig. 3(a). In the reconstructed phase images, the direction and the density of white lines correspond to the direction and the density of lines of magnetic flux projected along the electron beam, respectively. It is known that the constant flux of $h/e(= 4.1 \times 10^{-15}$ Wb) flows between two adjacent white lines [7], where h and e are Planck's constant and the elementary electric charge, respectively. Thus, the magnetic flux density (B) at some point can be evaluated by the relation $B = h/(\mathrm{etd})$, where t is the specimen thickness and d is the distance between the white lines or the black lines in the reconstructed phase image. With the increase in magnetic field, domain walls like fishbone start to disappear, as shown in Fig. 3(c)–(d). Further, it should be noted that the magnetic flux density in the region marked with an asterisk in Fig. 3(a) increases with the increase in magnetic field. The magnetic flux density in Fig. 3(a) and (d) are evaluated to be approximately 0.06 and 0.11 T, respectively. Thus, we consider that these regions correspond to the mixed-phase state of ferromagnetic and superparamagnetic phases. This situation is rather consistent with the magnetization curve of Fig. 2(b), which shows somewhat superparamagnetic behavior.

Fig. 4(a) and (b) shows a Lorentz microscope image and a reconstructed phase image of the same area in $Co_{34.4}Pt_{13.5}Al_{15.6}O_{36.5}$ thin film. As we mentioned earlier, no magnetic

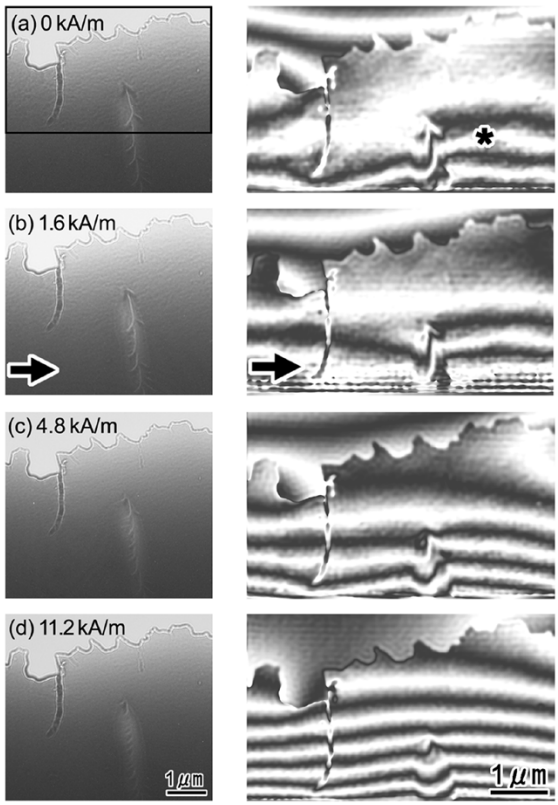

Fig. 3. Lorentz microscope images (left parts) and the reconstructed phase images (right parts) of $Co_{38.7}Pt_{15.6}Al_{16.3}O_{29.4}$ thin film obtained when the magnetic fields applied are 0, 1.6, 4.8, and 11.2 kA/m, respectively. The black arrows indicate the direction of the magnetic fields applied. The phase amplification is 1.

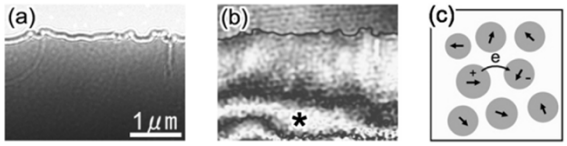

Fig. 4. (a) Lorentz microscope image (over) and (b) the reconstructed phase image of the same area in $Co_{34.4}Pt_{13.5}Al_{15.6}O_{36.5}$ thin film. (c) Schematic illustration showing the superparamagnetic state. The phase amplification is 2.

domain walls are observed since the magnetization direction in each nanocrystalline phase are random, as illustrated schematically in Fig. 4(c). This superparamagnetic state can be explained with the formula $k_BT \approx KV/25$ [12]; that is, comparing with the energy barrier KV, the thermal vibration k_BT cannot be neglected, resulting in the free rotation of magnetization in each nanocrystalline phase. It is noted that in Fig. 4(b), the lines of magnetic flux are slightly fluctuated and the magnetic flux density is considerably low. By electron energy-loss spectroscopy (EELS), the thickness in the region indicated by the asterisk in Fig. 4(b) was roughly estimated to be 135 nm. Thus, the magnetic flux density in that region is evaluated to be approximately 0.03 T, which may result from the residual magnetic field of about 1.6 kA/m in TEM. The fluctuated lines of magnetic flux are considered to reflect the randomly magnetized distribution of CoPt-based single domain particles, as shown in Fig. 4(c). Meanwhile, it is noted that the $Co_{34.4}Pt_{13.5}Al_{15.6}O_{36.5}$ exhibits the extremely large electrical resistivity above 10^5 $\mu\Omega$·cm and the MR value of about 3% under an applied magnetic field of 560 kA/m at room temperature. Thus, it is reasonably considered that in the $Co_{34.4}Pt_{13.5}Al_{15.6}O_{36.5}$ thin film, the electrical conduction occurs by the spin-dependent tunneling of electrons since the probability of electron tunneling increases by the applied magnetic filed. In this superparamagnetic thin film, detailed analysis of lines of magnetic flux under a strong magnetic field produced by a sharp magnetic needle [13] is still in progress and the results will be published elsewhere.

ACKNOWLEDGMENT

This work was supported by a Grant-in-Aid for Scientific Research from the Ministry of Education, Science, Sports and Culture of Japan, and by the Special Coordination Funds for Promoting Science and Technology of "Nanohetero Metallic Materials" from the Science and Technology Agency.

REFERENCES

[1] H. Karamon, T. Masumoto, and Y. Makino, "Magnetic and electrical properties of Fe-B-N amorphous films," *J. Appl. Phys.*, vol. 57, pp. 3527–3532, Apr. 1985.
[2] H. Fujimori, S. Mitani, and S. Ohnuma, "Tunnel-type GMR in metal-nonmetal granular alloy thin films," *Mater. Sci. Eng. B*, vol. 31, pp. 219–223, 1995.
[3] M. Watanabe, T. Masumoto, D. H. Ping, and K. Hono, "Microstructure and magnetic properties of FePt-Al-O granular thin films," *Appl. Phys. Lett.*, vol. 76, pp. 3971–3973, May 2000.
[4] K. Hono and M. Ohnuma, "Microstructures and properties of nanocrystalline and nanogranular magnetic materials," in *Magnetic Nanostructures*, H. S. Nalwa, Ed: American Scientific, 2002, pp. 327–358.
[5] M. Ohnuma, K. Hono, E. Abe, H. Onodera, S. Mitani, and H. Fujimori, "Microstructure of Co-Al-O granular thin films," *J. Appl. Phys.*, vol. 82, pp. 5646–5652, Dec. 1997.
[6] D. Shindo, Y.-G. Park, Y. Murakami, Y. Gao, H. Kanekiyo, and S. Hirosawa, "Electron holography of Nd-Fe-B nanocomposite magnets," *Scripta Mater.*, vol. 48, pp. 851–856, 2003.
[7] D. Shindo and T. Oikawa, *Analytical Electron Microscopy for Materials Science*. Tokyo, Japan: Springer-Verlag, 2002, pp. 116–118.
[8] S. Chikazumi, *Physics of Ferromagnetism*, 2nd ed. Oxford, U.K.: Clarendon, 1997, pp. 428–432.
[9] W. Szmaja, "The thickness dependence of the magnetic domain structure in cobalt monocrystals studied by SEM," *J. Magn. Magn. Mater.*, vol. 153, pp. 215–223, 1996.
[10] Y. Zhu and M. R. McCartney, "Magnetic-domain structure of $Nd_2Fe_{14}B$ permanent magnets," *J. Appl. Phys.*, vol. 84, pp. 3267–3272, Sep. 1998.
[11] Z. Liu, D. Shindo, S. Ohnuma, and H. Fujimori, "Nano-granular Co-Zr-O magnetic films studied by HRTEM and electron holography," *J. Magn. Magn. Mater.*, vol. 262, pp. 308–315, 2003.
[12] I. S. Jacobs and C. P. Bean, "Fine particles, thin films and exchange anisotropy," in *Magnetism*, G. T. Rado and H. Suhl, Eds. New York: Academic, 1963, vol. III, pp. 271–350.
[13] H. S. Park, Y.-G. Park, Y. Gao, D. Shindo, and M. Inoue, "Direct observation of magnetization reversal in thin $Nd_2Fe_{14}B$ film," *J. Appl. Phys.*, vol. 97, pp. 033 908-1–033 908-4, Feb. 2005.

Manuscript received January 31, 2005.